Journal of Alloys and Compounds 512 (2012) 216–222

Contents lists available at SciVerse ScienceDirect

Journal of Alloys and Compounds

journal homepage: www.elsevier.com/locate/jallcom

Synthesis and characterization of sol–gel derived gallium-doped zinc oxide thin films

Chien-Yie Tsay[a,*], Kai-Shiung Fan[a], Chien-Ming Lei[b]

[a] Department of Materials Science and Engineering, Feng Chia University, Taichung 407, Taiwan, ROC
[b] Department of Chemical and Materials Engineering, Chinese Culture University, Taipei 111, Taiwan, ROC

ARTICLE INFO

Article history:
Received 2 November 2010
Received in revised form
20 September 2011
Accepted 22 September 2011
Available online 29 September 2011

Keywords:
Transparent oxide semiconductor
GZO thin films
Sol–gel method
X-ray photoelectron spectroscopy
Photoluminescence

ABSTRACT

Gallium-doped ZnO (GZO) semiconductor thin films were prepared by a sol–gel spin coating process. The effects of Ga dopant concentrations on the microstructure, electrical resistivity, optical properties, and photoluminescence (PL) were studied. XRD results showed that all the as-prepared GZO films had a wurtzite phase and a preferred orientation along the [0 0 2] direction. ZnO thin films doped with Ga had lower electrical resistivity, lower RMS roughness, and improved optical transmittance in the visible region. The lowest average electrical resistivity value, $2.8 \times 10^2\ \Omega\,cm$, was achieved in the ZnO thin films doped with 2% Ga, which exhibited an average transmittance of 91.5%. This study also found that the optical band gap of Ga-doped films was 3.25 eV, slightly higher than that of undoped samples (3.23 eV), and the PL spectra of GZO films showed strong violet-light emission centers at about 2.86 eV (the corresponding wavelength of which is about 434 nm).

© 2011 Elsevier B.V. All rights reserved.

1. Introduction

Transparent metal oxide thin films have been widely used in optoelectronic devices (such as touch screens, flat panel displays, and thin-film solar cells) because of the combination of excellent electrical properties and high transparency [1–3]. Among the varieties of films, zinc oxide (ZnO) based transparent conducting/semiconducting thin films are attracting great attention because they are promising candidates for transparent and flexible electronics [4,5]. Polycrystalline ZnO-based semiconductor thin films have higher carrier mobility, greater chemical stability, and lower photosensitivity levels than conventional hydrogenated amorphous silicon (a-Si:H) thin films. Therefore, they can replace a-Si:H thin films as the active channel layers in TFTs to improve electrical performance [6–10]. Recently, it has also been demonstrated that they can be used in transparent memory [11,12].

Group III (B, Al, Ga, In, etc.) and group IV (Si, Ge, Sn, Ti, Zr, etc.) elements have been used as effective donors to enhance the electrical and optical properties of ZnO films [2,13–17]. Dopant atoms incorporated into a ZnO crystal lattice replace Zn host atoms; however, such incorporation may induce lattice distortion and degrade crystallinity. The ionic radius of Ga^{3+} (0.62 Å) is smaller than that of Zn^{2+} (0.74 Å), which allows easy substitution of Ga^{3+} for Zn^{2+}; in addition, the covalent band length of Ga–O (1.92 Å) is slightly shorter than that of Zn–O (1.97 Å), which reduces lattice distortion in ZnO thin films [8,18]. Therefore, of all the group-III elements considered for use as substitutional dopants in ZnO thin films, Ga could be the best candidate because of its lower reactivity and greater resistance to oxidation, the combination of which leads to greater electronegativity than possible with other dopants [19,20].

Ga-doped ZnO thin films have been prepared with vacuum deposition techniques such as RF magnetron sputtering [13,18,19], pulsed laser deposition (PLD) [15,21], and metal–organic chemical vapor deposition (MOCVD) [22], and with chemical solution deposition processes such as sol–gel process [8,16,20] and spray pyrolysis [23,24]. The sol–gel method, a wet chemical process, is an alternative to vacuum deposition techniques that offers simplicity, cost effectiveness, and a large-area thin-film coating.

Most previous studies have focused on the development of GZO transparent conducting oxide (TCO) thin films for display and solar cell applications. For example, Yamamoto et al. reported the word's first 20-inch liquid crystal display television (LCD-TV), which had a GZO transparent electrode prepared on an RGB color filter using dc magnetron sputtering [25]. Wong et al. grew GZO thin films at room temperature by pulsed laser deposition [26]. Those films, which have excellent transparency and conductivity, can be used as electrodes in organic devices. However, few studies have focused on the characteristics of sol–gel derived GZO semiconductor thin films [8,27]. Therefore, it is worthwhile to systematically study the properties of transparent GZO semiconductor thin films for further application in transparent electronics. In this study, the authors investigated the structural characteristics,

* Corresponding author. Tel.: +886 4 24517250x5312; fax: +886 4 24510014.
E-mail address: cytsay@fcu.edu.tw (C.-Y. Tsay).

0925-8388/$ – see front matter © 2011 Elsevier B.V. All rights reserved.
doi:10.1016/j.jallcom.2011.09.066

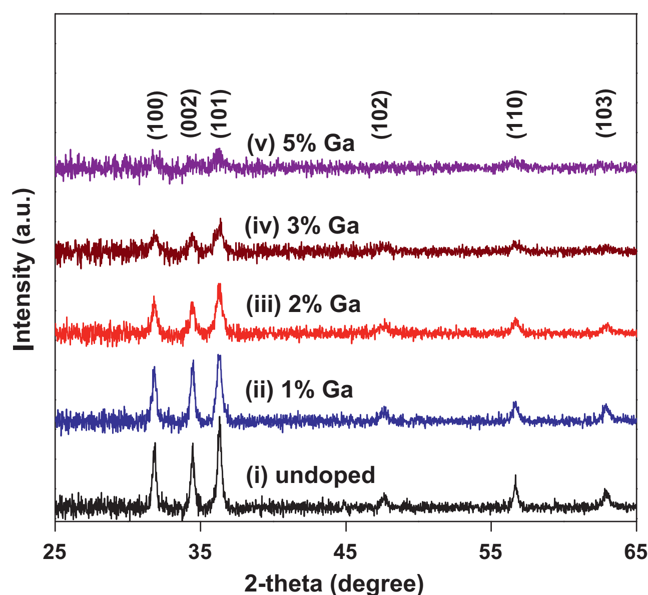

Fig. 1. XRD patterns of ZnO thin films doped with different Ga concentrations.

electrical resistivity, optical properties, and photoluminescence of GZO semiconductor thin films fabricated by sol–gel process.

2. Experimental procedures

The precursor solutions for spin coating were synthesized by dissolving zinc acetate dihydrate (J.T. Baker, 99.2% purity) and gallium nitrate hydrate (Aldrich, 99.999% purity) in a 2-methoxyethanol (2-ME, Alfa Aesar, 99.0% purity) solvent, and then a monoethanolamine (MEA, J.T. Baker, 99.7% purity) stabilizer was added to the mixed solution [8]. The Ga dopant concentration ([Ga]/[Zn + Ga]) was varied from 0 to 5 at.%. The concentration of metal ions in each solution was 0.25 M, and the molar ratio of MEA to metal ions was maintained at 1.0. Each solution was stirred at 60 °C for 2 h, yielding clear, transparent solutions. The resulting solutions were aged for 120 h at room temperature before application as coating solutions. The glass substrates were cleaned in IPA (isopropyl alcohol) and ethanol for 10 min at each step using an ultrasonic cleaning process. The ultrasonic cleaning process was followed by a deionized (DI) water washing process, after which the glass was immediately dried by being sprayed with nitrogen gas [20].All Ga-doped ZnO sol–gel films were spin-coated onto pre-cleaned alkali-free OA-10 glass (Nippon Electric Glass Co., Ltd.) at a rotation speed of 1000 rpm for 30 s. Each coated film was dried at 200 °C for 10 min. After the spin coating and drying procedures were repeated once, the sol–gel films were annealed in ambient air at 500 °C for 2 h in a quartz tube furnace. The crystal structure and crystallinity of the annealed Ga-doped ZnO (GZO) thin films were determined by glancing angle X-ray diffraction (GAXRD). These diffraction patterns were examined with a Bruker D8 SSS X-ray diffractometer using CuKα radiation (λ = 1.5406 Å) with a glancing incident angle of 0.8° and a step size of 0.02°/s. Plane-view and cross-sectional view micrographs of the GZO thin films were acquired by field-emission scanning electron microscopy (FE-SEM, Hitachi S-4800). The microstructure of the 2% Ga-doped ZnO thin film was characterized by transmission electron microscopy (TEM, FEI Tecnai G2 F20). The surface morphologies and surface roughness levels of the films were determined by tapping mode scanning probe microscopy (SPM, Digital Instrument NS4/D3100CL/MultiMode) with a scan area of 1 μm × 1 μm. Electrical resistivity was determined from sheet resistance and film thickness. The sheet resistance of each GZO thin film was measured with a contact-type resistive meter (Mitsubishi Chemical Co. MCP-HT450). Transmittance spectra of these films were recorded with a UV–vis spectrophotometer (Hitachi U-2900). The composition and chemical bonds of undoped and Ga-doped samples were determined by X-ray photoelectron spectroscopy (XPS, Thermo Scientific K-Alpha). Before XPS measurement was performed, the surfaces of the films were polished by Ar ion sputtering for 10 s. A Jobin-Yvon Triax 550 monochromator and a He–Cd laser (λ = 325 nm) were used for photoluminescence (PL) studies.

3. Results and discussion

Fig. 1 shows the XRD patterns of undoped and Ga-doped ZnO thin films annealed at 500 °C for 2 h. XRD results showed that all as-prepared films were polycrystalline, with a hexagonal wurtzite structure, and the XRD pattern of each sample indicated the relatively higher diffraction intensity of the (1 0 1) plane. These diffractographs also showed that the intensities of these diffraction peaks tended to decrease with increasing Ga dopant concentrations. The diffraction signals of the (1 0 2) and (1 0 3) planes were very weak, with Ga dopant concentrations in excess of 3% (curves (iv) and (v) in Fig. 1). These findings indicate at higher Ga doping levels, the crystalline qualities of the ZnO thin films were degraded. Nishino et al. reported that this degradation may be caused by the influence of stresses arising from the difference in the ionic radii of zinc and the dopant [28]. Moreover, the XRD patterns indicated that the 5% Ga-doped ZnO thin films had a rather amorphous nature.

Table 1
The variation of the texture coefficient of GZO thin films with Ga dopant concentration.

Ga dopant concentration (%)	Texture coefficient ($TC_{(hkl)}$)					
	(1 0 0)	(0 0 2)	(1 0 1)	(1 0 2)	(1 1 0)	(1 0 3)
0	1.12	1.53	0.95	0.67	1.06	0.68
1	1.18	1.71	0.82	0.79	0.76	0.74
2	1.22	1.33	0.93	0.91	0.93	0.69
3	0.85	1.22	0.94	1.03	0.96	–
5	0.83	0.99	0.76	–	1.41	–

The preferred growth orientation of polycrystalline thin films can be understood from the texture coefficient $TC_{(hkl)}$ for all planes. The texture coefficient of the (hkl) plane is calculated using the following equation [23,29]:

$$TC_{(h\ kl)} = \left(\frac{I_{(hkl)}/I_{r(hkl)}}{[1/n \sum I_{(hkl)}/I_{r(hkl)}]} \right) \quad (1)$$

where $I_{(khl)}$ is the XRD intensity obtained from the films, n is the number of diffraction peaks considered, and $I_{r(khl)}$ is the intensity of the reference XRD patterns (JCPDS card 36-1451). Table 1 shows the variation in texture coefficient of the series of GZO thin films with Ga dopant concentration. The relatively higher values of texture coefficient are along the (0 0 2) plane for all of the films. This indicates that the GZO thin films had a preferential orientation along the (0 0 2) plane.

Doping ZnO thin films with Ga increased the full widths at half maximum (FWHMs) of the (1 0 0), (0 0 2), and (1 0 1) peaks, indicating that Ga doping reduced the crystallite size of the GZO thin films. The crystallite sizes of the films were estimated by Scherrer's formula. The average crystallite sizes of undoped and 1% Ga-doped ZnO thin films, for the three main diffraction peaks of the (1 0 0), (0 0 2), and (1 0 1) planes, were 24.3 and 20.8 nm, respectively. When the Ga dopant concentrations were increased from 2 to 5%, the average crystallite sizes decreased from 18.2 to 12.2 nm. Fig. 2 distinctly shows that the average crystallite sizes of GZO thin films decreased as dopant concentration increased. The corresponding microstructure feature can also be observed in the cross-sectional view SEM micrographs in Fig. 3. In that figure, the cross-sectional SEM images show that the polycrystalline GZO thin films had a nanoscale granular structure, and the average thickness of the films was about 65 nm. The particle size of those films observably decreased with increases in Ga dopant concentration, which was in agreement with XRD measurements. The Ga-doped ZnO thin films exhibited particle sizes finer than those of undoped ZnO films because the incorporation of Ga dopants into ZnO increased the number of nucleation sites [27,30].

Each inset image in Fig. 3 is the plane view SEM micrograph of a corresponding GZO thin film sample. The surfaces of the undoped ZnO thin films showed irregular fiber-like and wrinkle-like stripes (inset of Fig. 3(a)), indicating progressive dispersal as Ga dopant

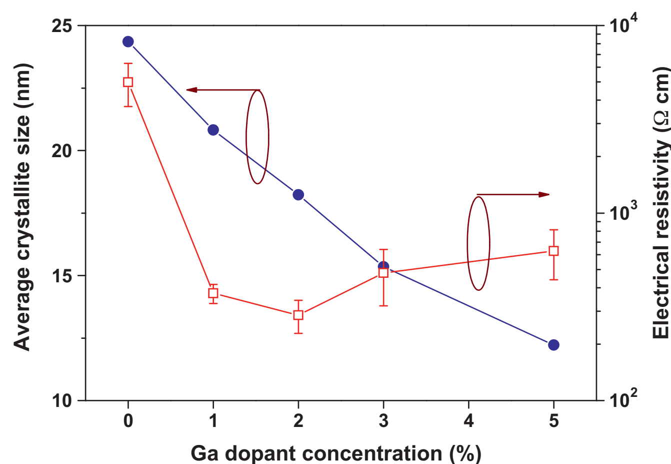

Fig. 2. Variation of average crystallite size and electrical resistivity of GZO thin films with Ga concentration.

levels increased from 1 to 5%. The surfaces of 5% Ga-doped ZnO thin films did not have that appearance, as can be seen from the SEM micrograph of the surface of the film (inset of Fig. 3(e)). When a synthesizing process for a ZnO sol induces a substantial loss of OR (hydroxy or alkoxy) groups, surfaces of sol–gel derived ZnO thin films tend to exhibit fiber-like stripes and wrinkles. Thus, a relatively flat surface can be produced if the starting materials supply enough OR groups [31].

Fig. 4 shows a plane-view TEM micrograph of the 2% Ga-doped ZnO thin film, in which nanoscale particle sizes can be observed. Moreover, the selected area electron diffraction (SAED) pattern (inset of Fig. 4) shows discontinuous diffraction rings, which indicate that the film is nanocrystalline. TEM results are the aggregation of XRD analysis and SEM observation.

The electrical resistivity of doped ZnO thin films is strongly affected by the preparation processes, chemical compositions, microstructures, and annealing atmosphere. The resistivity of each GZO thin film was calculated by multiplying the sheet resistance by the film thickness. Variations in the electrical resistivity of GZO thin films with Ga concentrations are shown in Fig. 2. That figure shows that Ga-doped films had lower average electrical resistivity values than did undoped films, and that resistivity values decreased with Ga dopant concentrations of up to 2% but increased with

Fig. 3. Cross-sectional SEM micrographs of GZO thin films: (a) undoped, (b) 1%, (c) 2%, (d) 3%, and (e) 5% Ga-doped samples. Each inset image is a plane view SEM micrograph of the corresponding thin film sample.

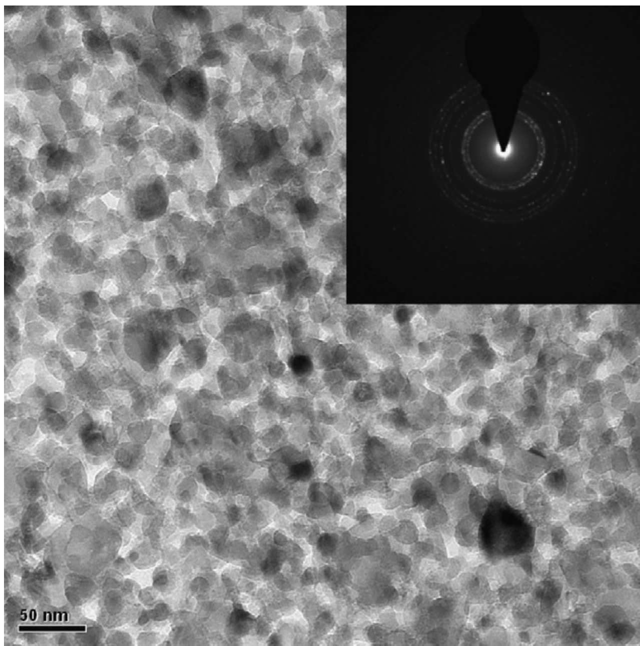

Fig. 4. Plane-view TEM micrograph of the 2% Ga-doped ZnO thin film. The inset image is a SAED pattern of the corresponding thin film sample.

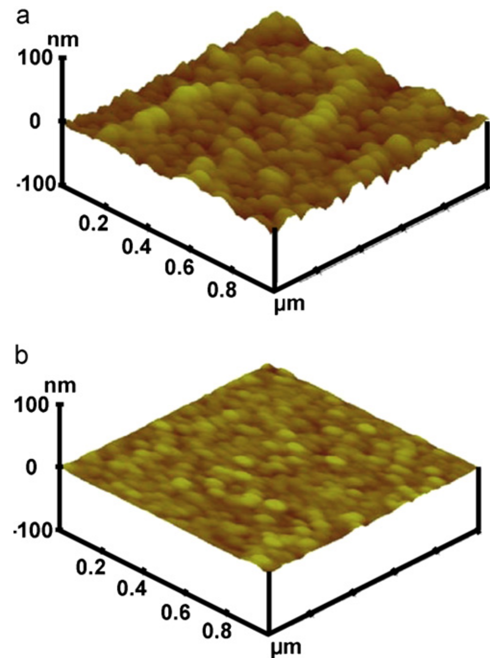

Fig. 5. SPM images of GZO thin films: (a) undoped and (b) 5% Ga-doped samples.

concentrations greater than that. That is, the 2% Ga-doped ZnO thin films exhibited the lowest average resistivity, $2.8 \times 10^2\ \Omega$ cm, among all of the annealed GZO thin films investigated in this study. The decrease in resistivity of GZO thin films with Ga dopant concentrations of up to 2% was due to an increase in carrier concentration attributed to the contribution of the dopant ions. However, the resistivity of GZO thin films increased with dopant concentrations higher than 2% because those films possessed a greater number of grain boundaries due to the smaller grain size and degraded crystallinity, which caused the carrier concentration to decrease due to carrier traps at the grain boundaries and carrier scattering by crystal defects.

Two SPM images of GZO thin films (taken from undoped and 5% Ga-doped samples) are shown in Fig. 5. The undoped sample had an observable granular configuration, and many particles were arranged into strips (Fig. 5(a)). However, the 5% Ga-doped thin film, which did not have a strip-like configuration, exhibited a finer particle size than that of the undoped thin film (Fig. 5(b)). The significant improvement in surface flatness of ZnO thin films doped with 5% Ga is notable. Fig. 6 shows that the RMS roughness of GZO thin films decreased with Ga dopant concentrations of up to 5%. This decrease indicates that the 5% Ga-doped samples had the smallest RMS value, 1.17 nm. It is widely believed that the RMS roughness levels of metal oxide films are directly related to their average crystallite sizes [32].

The optical transmittance spectra of undoped and Ga-doped thin films in ultraviolet and visible ranges are shown in Fig. 7. All transmittance spectra showed sharp absorption edges in the wavelength region between 360 and 400 nm, and those absorption edges shifted toward shorter wavelengths (blue shifted) when Ga was incorporated into the ZnO films. Similar behavior was also observed by Rao et al. for GZO transparent conducting thin films prepared by spray pyrolysis technique [23]. The magnitudes of the shifts increased in proportion to the amount of Ga. Furthermore, all Ga-doped samples exhibited higher transparency than the undoped ZnO sample (Fig. 7). The average transmittance values of GZO thin films were calculated for wavelengths of 500–800 nm. GZO thin films with Ga dopant levels over 2% exhibited average transmittance values over 91%, and the 3% Ga-doped thin films had the best average transmittance, 92.1%. Lee et al. reported that the optical properties of sol–gel derived ZnO films were mainly affected by surface morphology [33]. The transmittance of the ZnO thin films in the visible light region was also affected by film thickness, grain size, and defects (such as nanopores and nanovoids). The transmittance of the doped films with 5% Ga was lower than that of the 3% Ga films (Fig. 7). That result may be due to degradation of film quality (curve (v) in Fig. 1) and increased numbers of nanopores in the films (Fig. 3(e)) caused by the high Ga doping level.

The optical band gaps were obtained from the optical transmission spectra by plotting α^2 versus $h\nu$ and extrapolating the strain lines portion of this plot to the photon energy axis (Fig. 7(b)). The absorption coefficient (α) and photon energy ($h\nu$) can be related by the following expression,

$$\alpha = \frac{A(h\nu - E_g)^{m/2}}{h\nu} \quad (2)$$

where $m = 1$ for direct transition, $m = 4$ for indirect transition, E_g is the optical band gap, and A is a constant. The transitions in ZnO thin

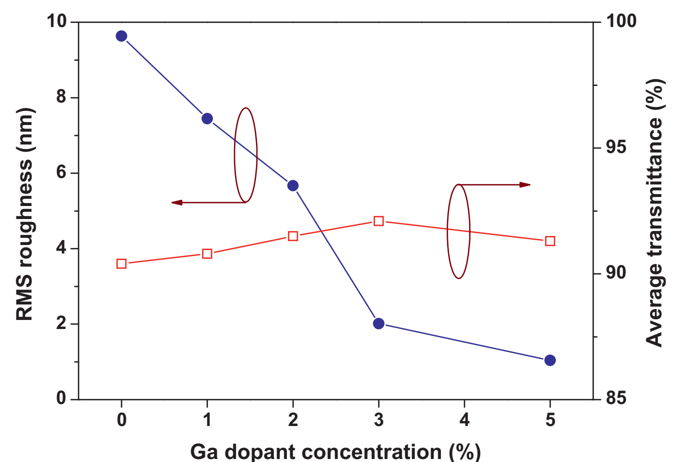

Fig. 6. Variation of RMS roughness and average transmittance of GZO thin films with Ga concentration.

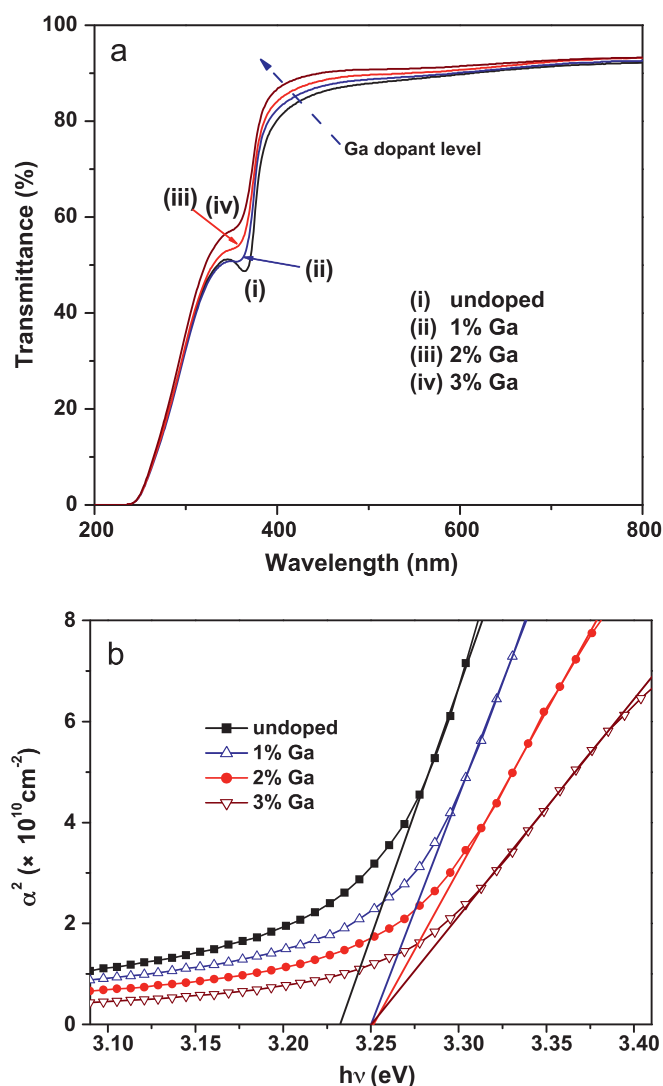

Fig. 7. (a) Optical transmittance spectra and (b) plot of α^2 versus $h\nu$ for undoped and Ga-doped thin films.

films are direct in nature. The absorption coefficient (α) was calculated using $\alpha = (1/t)\ln[1/T]$, where t is the film thickness and T is transmittance. The E_g value of undoped ZnO thin films was 3.23 eV, which is the same as in our previous report [31], and the E_g value of Ga-doped samples was 3.25 eV, slightly higher than that of undoped samples. The optical band gap blue shift for doped ZnO thin films is due to the increase in the density of carrier concentration, which leads to broadening of the energy band [20,23]. Kalaivanan et al. proposed that the broadening of the optical band gap could be ascribed mainly to the increase in disordering of polycrystalline semiconductor films, which leads to the appearance of localized electron and hole states [34]. Such a transparent oxide semiconductor (TOS) thin film could be applied as an active channel layer in transparent thin film transistors (TTFTs).

XPS was used to identify the chemical bonding states and to examine the relative atomic composition of chemical elements in Ga-doped ZnO thin films. Fig. 8 shows XPS spectra taken from the Ga, Zn, and O regions of undoped and Ga-doped samples. The undoped ZnO sample shows only Zn and O peaks. Fig. 8(a) shows the Ga 2p XPS spectra, which do not show observable shifts with different Ga doping levels, and peaks located at 1118.2 eV and 1145.2 for the 2% and 5% Ga-doped samples, which correspond to the electronic states of Ga $2p_{3/2}$ and Ga $2p_{1/2}$ (curves (ii) and (iii) in Fig. 8(a)),

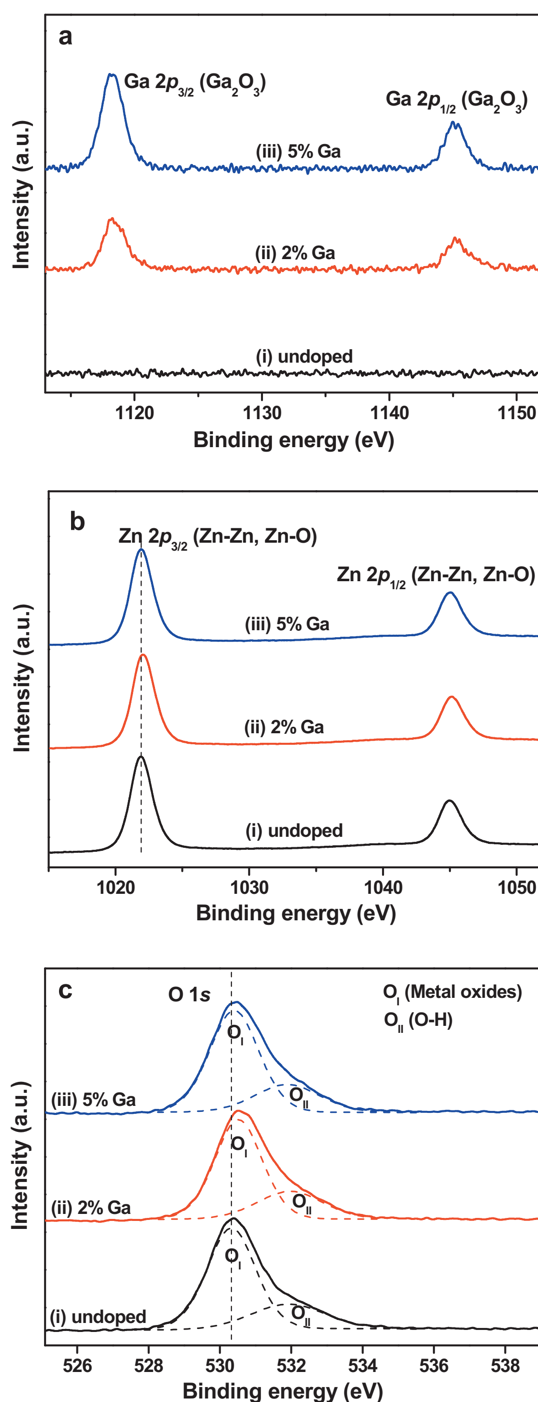

Fig. 8. XPS analysis of GZO thin films: (a) Ga region, (b) Zn region, and (c) O region.

respectively. The Ga $2p_{3/2}$ peak at 1118.2 eV, which is closer to the reported value of 1117.5 eV [35], is attributed to Ga^{3+} in Ga_2O_3. In addition, the peak height of Ga $2p_{3/2}$ and Ga $2p_{1/2}$ tended to increase with increasing Ga dopant concentration, indicating an increase in the concentration of Ga introduced into ZnO.

In Fig. 8(b), the Zn 2p spectra do not show observable shifts with increases in the Ga dopant concentration. However, when the Ga dopant was introduced into ZnO, the O 1s spectra shifted slightly toward a higher binding energy (Fig. 8(c)). Yoshino et al. reported XPS results indicating that the chemical shift of oxygen (1 s) for a sol–gel derived Ga-doped ZnO (GZO) thin film was smaller than the shifts of In- and Al-doped films [36]. This means that Ga ions can more easily replace Zn ions than In and Al ions can.

Table 2
The surface compositions of undoped and Ga-doped ZnO thin films, calculated from XPS measurements.

Ga dopant concentration (%)	Composition (at. %)		
	O	Zn	Ga
0	47.0	53.0	N.D.
1	46.1	53.0	1.0
2	45.9	52.7	1.4
3	46.7	51.8	1.5
5	46.0	51.6	2.4

The peaks at 1022.0 and 1045.2 eV for the 2% Ga-doped sample are the electronic states of Zn $2p_{3/2}$ and Zn $2p_{1/2}$ (curve (ii) in Fig. 8(b)). The location of the Zn $2p_{3/2}$ peak is very close to the reported value of 1021.7 eV [37], which is attributed to the Zn^{2+} ions in the ZnO (Zn–O and Zn–Zn bonds). From Fig. 8(c), it is noted that the O 1s spectra are asymmetric, and the peaks can be deconvoluted to two separate peaks, namely two kinds of oxygen species (O_I and O_{II}). The dashed lines in Fig. 8(c) show Gaussian fits to the experimental data (solid lines). The O_I peak (about 530.3 eV) is attributed to the O^{2-} ions in the ZnO crystal lattice, which corresponds to O–M bonds (metal oxides), and the O_{II} peak (about 531.9 eV) is attributed to chemisorbed or dissociated oxygen on surface hydroxyl, which corresponds to O–H bonds [38,39].

The stoichiometry of sol–gel derived GZO thin films, calculated from XPS results, is shown in Table 2. The data reveal that the ratio of O/(Zn + Ga) is smaller than the stoichiometric ratio 1:1, implying oxygen vacancies. From the listed data, it was also found that the Ga atomic compositions of as-prepared thin film samples were 1.0 at.%, 1.4 at.%, 1.5 at.%, and 2.4 at.% for 1%, 2%, 3%, and 5% Ga-doped samples, respectively. The actual atomic concentrations of gallium ([Ga]/[Zn + Ga]) incorporated in the films were different from the expected values. The probable explanation is that the concentration of interstitial Zn and Ga varied with Ga dopant concentration due to evaporation of Zn and/or Ga.

Normalized room-temperature PL spectra of nanocrystalline GZO thin films are shown in Fig. 9. These spectra, after Gaussian fitting, represent three bands: UV emission, violet emission, and green emission. The three types of PL bands shifted toward the short-wavelength when the ZnO thin films were doped with Ga. Yang et al. reported that the visible emission peak blue-shifted after Ga doping, which may be ascribed to the recombination with higher emission energy introduced by the Ga dopants [40].

Weak UV emission and strong violet emission were observed in all of the PL spectra. The undoped ZnO films present the UV emission center at 3.27 eV (Fig. 9(a)); the corresponding wavelength is about 379 nm, which is derived from the free excitonic recombination [41,42]. The violet emission and the green emission centers of undoped ZnO films were at 2.85 and 2.47 eV, respectively. According to Wei et al., the violet-light emission corresponds to the electronic transition from the shallow donor energy level of the Zn interstitials and doped Ga atoms to the top of the valence band level [43]. Børseth et al. assigned the green emission at 2.53 eV to oxygen vacancy-related defect levels [44]. Vanheusden et al. proposed that the mechanism for the green emission was the recombination of electrons in singly ionized oxygen vacancies with photoexcited holes in the valence band [45]. From the above discussion, it is concluded that the visible emission is strongly related to intrinsic defects in the nanocrystalline GZO thin films.

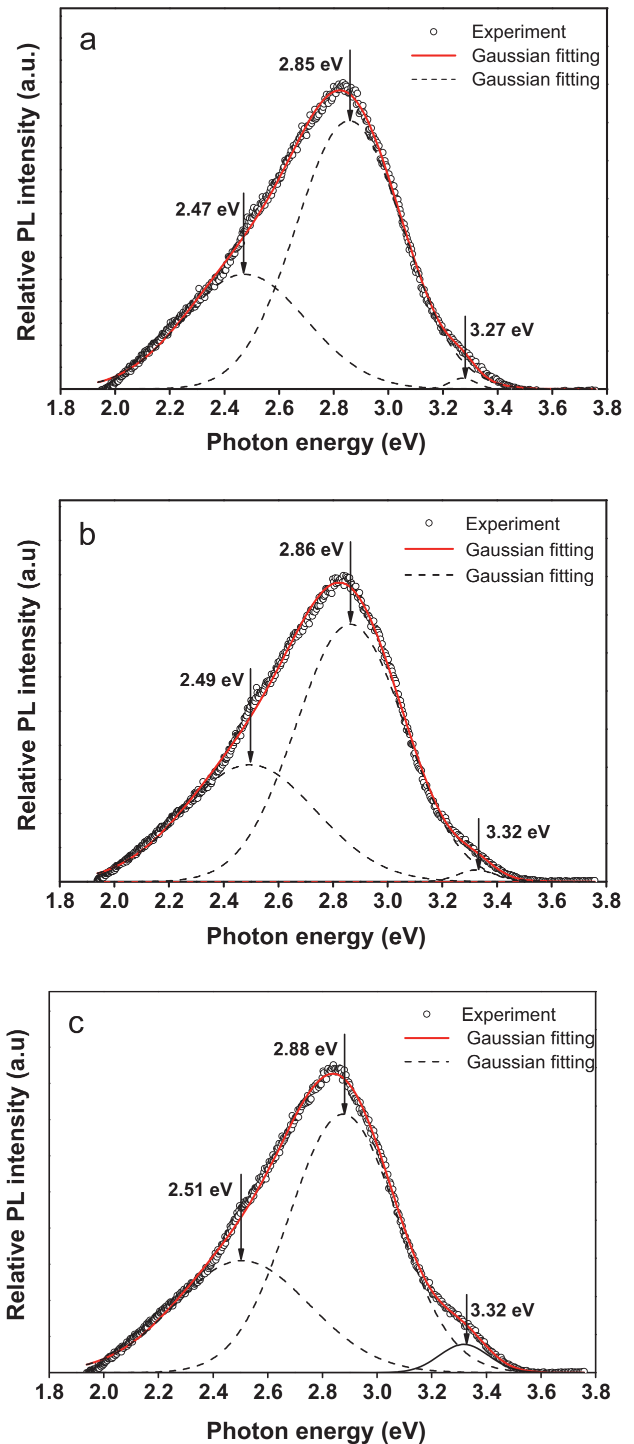

Fig. 9. Normalized room temperature PL spectra of GZO thin films: (a) undoped, (b) 2% Ga-doped, and (c) 5% Ga-doped samples.

4. Conclusions

We have successfully fabricated Ga-doped ZnO (GZO) transparent semiconductor thin films on alkali-free glass by sol–gel spin coating. All nanocrystalline GZO thin films had a hexagonal wurtzite structure and exhibited a preferential orientation along the (0 0 2) plane. Doping the ZnO thin films with Ga obviously reduced surface roughness, decreased electrical resistivity, improved transparency in the visible range, and refined the microstructure as compared to undoped ZnO thin films. The 2%

Ga-doped ZnO thin films exhibited the lowest average resistivity, $2.8 \times 10^2\ \Omega\,cm$, among all of the GZO thin films. The optimum microstructure characteristics, transparency, and resistivity of GZO films were attained with a Ga dopant level of 2%. Semiconductors employing this film can be used for transparent electronic devices.

Acknowledgment

The authors gratefully acknowledge the financial support of the National Science Council of the Republic of China under Contract No. NSC 96-2221-E-035-055-MY3.

References

[1] M. Grundmann, H. Frenzel, A. Lajn, M. Lorenz, F. Schein, H.V. Wenckstern, Phys. Status Solidi A 207 (2010) 1437–1449.
[2] T. Minami, Semicond. Sci. Technol. 20 (2005) S35–S44.
[3] H. Ohta, H. Hosono, Mater. Today 7 (2004) 42–51.
[4] A. Lu, J. Sun, J. Jiang, Q. Wan, Appl. Phys. Lett. 96 (2010) 043114.
[5] H.C. Cheng, C.Y. Tsay, J. Alloys Compd. 507 (2010) L1–L3.
[6] K. Remashan, Y.S. Choi, S.J. Park, J.H. Jang, J. Electrochem. Soc. 157 (2010) H60–H64.
[7] Y.H. Hwang, S.J. Seo, B.S. Bae, J. Mater. Res. 25 (2010) 695–700.
[8] W.J. Park, H.S. Shin, B.D. Ahn, G.H. Kim, S.M. Lee, K.H. Kim, H.J. Kim, Appl. Phys. Lett. 93 (2008) 083508.
[9] V.P. Verma, D.H. Kim, H. Jeon, M. Jeon, W. Choi, Thin Solid Films 516 (2008) 8736–8739.
[10] H. Jeon, V.P. Verma, S. Hwang, S. Lee, C. Park, D.H. Kim, W. Choi, M. Jeon, Jpn. J. Appl. Phys. 47 (2008) 87–90.
[11] K. Kinoshita, T. Okutani, H. Tanaka, T. Hinoki, H. Agura, K. Yazawa, K. Ohmi, S. Kishida, Solid State Electron. 58 (2011) 48–53.
[12] N.T. Salim, K.C. Aw, W. Gao, B.E. Wright, Thin Solid Films 518 (2009) 362–365.
[13] T. Minami, H. Sato, H. Nanto, S. Takata, Jpn. J. Appl. Phys. 24 (1985) L781–L784.
[14] H. Sato, T. Minami, S. Takata, J. Vac. Sci. Technol. A 11 (1993) 2975–2979.
[15] H. Kim, J.S. Horwitz, W.H. Kim, A.J. Mäkinen, Z.H. Kafafi, D.B. Chrisey, Thin Solid Films 420–421 (2002) 539–543.
[16] J.H. Lee, B.O. Park, Thin Solid Films 426 (2003) 94–99.
[17] M. Caglar, S. Ilican, Y. Caglar, F. Yakuphanoglu, J. Alloys Compd. 509 (2011) 3177–3182.
[18] V. Assunção, E. Fortunato, A. Marques, A. Gonçalves, I. Ferreira, H. Águas, R. Martins, Thin Solid Films 442 (2003) 102–106.
[19] J.H. Lee, Y.Y. Kim, H.K. Cho, J.Y. Lee, J. Cryst. Growth 311 (2009) 4641–4646.
[20] P.K. Nayak, J. Yang, J. Kim, S. Chung, J. Jeong, C. Lee, Y. Hong, J. Phys. D: Appl. Phys. 42 (2009) 035102.
[21] V. Bhosle, J.T. Prater, F. Yang, D. Burk, S.R. Forrest, J. Narayan, J. Appl. Phys. 102 (2007) 023501.
[22] J.H. Park, C.B. Lee, I.S. Kim, S.J. Jang, B.T. Lee, Thin Solid Films 517 (2009) 4432–4435.
[23] T.P. Rao, M.C.S. Kumar, J. Alloys Compd. 506 (2010) 788–793.
[24] A.R. Babar, P.R. Deshamukh, R.J. Deokate, D. Haranath, C.H. Bhosale, K.Y. Rajpure, J. Phys. D: Appl. Phys. 41 (2008) 135404.
[25] N. Yamamoto, H. Makino, S. Osone, A. Ujihara, T. Ito, H. Hokari, T. Maruyama, T. Yamamoto, Thin Solid Films, in press.
[26] L.M. Wong, S.Y. Chiam, J.Q. Huang, S.J. Wang, W.K. Chim, J.S. Pan, Sol. Energy Mater. Sol. Cells 95 (2011) 2400–2406.
[27] K.Y. Cheong, N. Muti, S.R. Ramanan, Thin Solid Films 410 (2002) 142–146.
[28] J. Nishino, S. Ohshio, K. Kamata, J. Am. Ceram. Soc. 75 (1992) 3469–3472.
[29] R. Romero, D. Leinen, E.A. Dalchiele, J.R. Ramos-Barrado, F. Martín, Thin Solid Films 515 (2006) 1942–1949.
[30] Y. Ohya, H. Saiki, T. Tanaka, Y. Takahashi, J. Am. Ceram. Soc. 79 (1996) 825–830.
[31] C.Y. Tsay, H.C. Cheng, Y.T. Tung, W.H. Tuan, C.K. Lin, Thin Solid Films 517 (2008) 1032–1036.
[32] J. Weng, Y. Zhang, G. Han, Y. Zhang, L. Xu, J. Xu, X. Huang, K. Chen, Thin Solid Films 478 (2005) 25–29.
[33] J.H. Lee, K.H. Ko, B.O. Park, J. Cryst. Growth 247 (2003) 119–125.
[34] A. Kalaivanan, S. Perumal, N.N. Pillai, K.R. Murali, Mater. Sci. Semicond. Process. 14 (2011) 94–96.
[35] A.E. Rakhshani, A. Bumajdad, J. Kokaj, S. Thomas, Appl. Phys. A 97 (2009) 759–764.
[36] K. Yoshino, T. Hata, T. Kakeno, H. Komaki, M. Yoneta, Y. Akaki, T. Ikari, Phys. Stat. Sol. (c) (2003) 626–630.
[37] C.D. Wagner, W.M. Riggs, L.E. Davis, J.F. Moulder, G.E. Muilenberg, Handbook of X-ray Photoelectron Spectroscopy, Perkin-Elmer Corp., Eden Prairie, Minnesota, USA, 1979, p. 84.
[38] M. Futsuhara, K. Yoshioka, O. Takai, Thin Solid Films 322 (1998) 274–281.
[39] C. Xu, G. Xu, Y. Liu, G. Wang, Solid State Commun. 122 (2002) 175–179.
[40] Y. Yang, J. Qi, Q. Liao, Y. Zhang, X. Yan, Y. Huang, L. Tang, Appl. Phys. A 94 (2009) 799–803.
[41] A.F. Kohan, G. Ceder, D. Morgan, C.G. Van de Walle, Phys. Rev. B 61 (2000) 15019–15027.
[42] Y.C. Kong, D.P. Yu, B. Zhang, W. Fang, S.Q. Feng, Appl. Phys. Lett. 78 (2001) 407–409.
[43] X. Wei, B. Man, C. Xue, C. Chen, M. Liu, Jpn. J. Appl. Phys. 45 (2006) 8586–8591.
[44] T.M. Børseth, B.G. Svensson, A.Y. Kuznetsov, P. Klason, Q.X. Zhao, M. Willander, Appl. Phys. Lett. 89 (2006) 262112.
[45] K. Vanheusden, W.L. Warren, C.H. Seager, D.R. Tallant, J.A. Voigt, B.E. Gnade, J. Appl. Phys. 79 (1996) 7983–7990.